Journal of Applied Sciences

ISSN 1812-5654

science alert

ANSInet
an open access publisher
http://ansinet.com

Journal of Applied Sciences 10 (14): 1369-1379, 2010
ISSN 1812-5654

Investigation of the Effects of Natural Gas Equivalence Ratio and Piston Bowl Flow Field on Combustion and Pollutant Formation of a DI Dual Fuel Engine

[1]A. Ghasemi and [2]M.H. Djavareshkian
[1]Department of Mechanical Engineering, University of Tabriz, Tabriz, Iran
[2]Department of Mechanical Engineering, Ferdowsi University of Masshhad, Masshhad, Iran

Abstract: The objective of this study is to simulate combustion process, pollutant formation and flow field in the combustion chamber of a DI diesel engine converted to work as a dual fuel (Diesel/Natural gas) engine. Effect of natural gas equivalence ratio, in constant diesel pilot injection and piston bowl shape, on the combustion process, pollutant formation and flow field are investigated in 5 cases defined. An eddy break-up combustion model and a diesel auto-ignition model were implemented to simulate the ignition and combustion processes. Experiments were performed on OM_355 DI diesel engine to validate the simulations. Results show that there have been good agreements between experiments and the CFD calculations.

Key words: Diesel engine, dual fuel, piston bowl, ignition, combustion

INTRODUCTION

The use of alternative gaseous fuels in engines for the production of power has been increasing worldwide. This has been prompted by the cleaner nature of their combustion compared with conventional liquid fuels as well as their relative increased availability at attractive prices. Their use in engine is expected to increase with the ever tightening of exhaust emission regulations.

Diesel engines, with appropriate relatively simple conversion, can be made to operate on gaseous fuels efficiently. Such engines, which are called dual fuel engines', usually have the gaseous fuel mixed with the air in the engine cylinders, either through direct mixing in the intake manifold with air or through injection directly into the cylinder. The resulting mixture after compression is then ignited through the injection of a small amount of diesel fuel (the pilot) in the usual way. This pilot liquid fuel can auto-ignite readily to provide ignition sources for subsequent flame propagation within the surrounding gaseous fuel mixture (Badr *et al*., 1999).

Most research in dual-fuel engines has concentrated on defining the extent of dual fueling and its effects on emissions and performance (Karim *et al*., 1993; Yasuhiro *et al*., 1995). A model was developed to simulate dual-fuel combustion by using a quasi-dimensional entrainment model (MZCM) for pilot jet combustion and conventional S.I. model for modeling of the combustion of premixed gas/air charge (Pirouzpanah and Kashani, 2000). In another research, a work was done, conducted to investigate the combustion characteristics of a dual fuel (Diesel-gas) engine at part loads using a single zone combustion model with detailed chemical kinetics for combustion of natural gas fuel (Pirouzpanah and Saray, 2007).

A multidimensional CFD model with a mixing controlled timescale combustion model has also been developed to study the diesel spray and natural gas combustion processes of a dual-fuel engine with success (Singh *et al*., 2004; Hountalas and Papagiannakis, 2001).

A new combustion model was developed and applied to simulate combustion in dual-fuel engines in which the premixed natural gas is ignited by the combustion flame initiated by a diesel spray. The model consists of a diesel auto-ignition model and a flame propagation model. A G-equation model previously developed to simulate SI engine combustion was incorporated with an auto-ignition model to simulate flame propagation in partially premixed environments (Satbir *et al*., 2006).

The objective of this work is multidimensional simulation of combustion process, pollutant formation and flow field in the combustion chamber of OM_355 DI diesel engine converted to work as a dual fuel (Diesel/Natural gas) engine, using Avl FIRE CFD tool. Effect of piston bowl shape, on the combustion process, pollutant formation and flow field are investigated. First the simulation is performed in complete diesel condition and then dual fuel combustion process is simulated. Results are validated by means of experiments performed on the above mentioned engine. Some results are also

Corresponding Author: M.H. Djavareshkian, Department of Mechanical Engineering, Ferdowsi University of Mashhad, P.O. Box 91775-1111, Mashhad, Iran Tel: +98-915-1095791 Fax: +98-511-8763304

compared to other research formerly done on the same engine by Pirouzpanah and Kashani (2000) who developed a code using a multizone combustion model (MZCM) in order to simulate diesel pilot jet combustion and a conventional S.I. combustion model for combustion of premixed gas/air charge.

MATERIALS AND METHODS

Computational fluis dynamics simulation

Basic equations: The conservation equations are presented for the following dynamic and thermodynamic properties (Djavareshkian and Ghasemi, 2009):

- Mass → Equation of continuity

$$\frac{\partial \rho}{\partial t} = -\frac{\partial}{\partial x_j}(\rho U_j) \tag{1}$$

- Momentum (Newton's second law) → Navier-Stokes equations

$$\frac{D(\rho U)}{Dt} = \frac{\partial(\rho U_i)}{\partial t} + \frac{\partial(\rho U_j U_i)}{\partial x_j} = \rho g_i - \frac{\partial P}{\partial x_i} + \frac{\partial}{\partial x_j}\left[\mu\left(\frac{\partial U_i}{\partial x_j} + \frac{\partial U_j}{\partial x_i} - \frac{2}{3}\frac{\partial U_k}{\partial x_k}\delta_{ij}\right)\right] \tag{2}$$

- Energy (1st Law of Thermodynamics) → Equation of energy

$$\frac{D(\rho H)}{Dt} = \frac{\partial(\rho H)}{\partial t} + \frac{\partial(\rho U_j H)}{\partial x_j} = \rho \dot{q}_g + \frac{\partial P}{\partial t} + \frac{\partial}{\partial x_i}\left(\tau_{ij} U_j\right) + \frac{\partial}{\partial x_j}\left(\lambda \frac{\partial T}{\partial x_j}\right) \tag{3}$$

- Concentration of species Equation

$$\frac{D(\rho C)}{Dt} = \frac{\partial(\rho C)}{\partial t} + \frac{\partial(\rho U_j C)}{\partial x_j} = \rho r + \frac{\partial P}{\partial t} + \frac{\partial}{\partial x_j}\left(D\frac{\partial C}{\partial x_j}\right) \tag{4}$$

Computational grid generation: Based on the geometry description, a set of computational meshes covering 360°CA was created. The 3D mesh of the modeled engine is shown in Fig. 1a, b, containing cylindrical (Cases 1-4) and OMEGA (Case_5) type piston bowls. A 90° sector mesh was used in this study considering that the diesel injector has four nozzle holes. This mesh resolution has been found to provide adequately independent grid results. The multi-block structure of the grid, containing spray and injector blocks, is shown in Fig. 2.

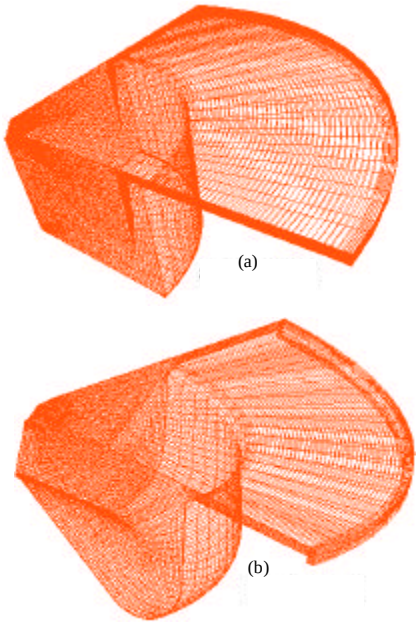

Fig. 1: 3-Dimensional grid of the modeled engine showing (a) cylindrical (Cases 1-4) and (b) OMEGA (Case_5) type piston bowls

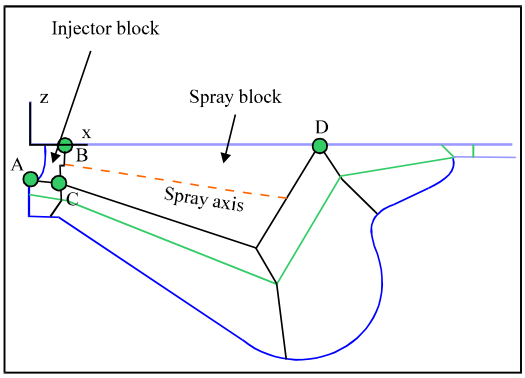

Fig. 2: Multi-block structure of the grid containing spray and injector blocks

Experimental setup, engine specifications and operating conditions: The OM_355 Mercedes Benz diesel engine is used in this study. Specifications and operating conditions of the engine are shown in Table 1 (Pirouzpanah and Saray, 2007). Two sets of experiments were Performed validation, one used diesel fuel only (Case_1) and the other used both diesel/natural gas dual fuels (Case_2). A schematic diagram of

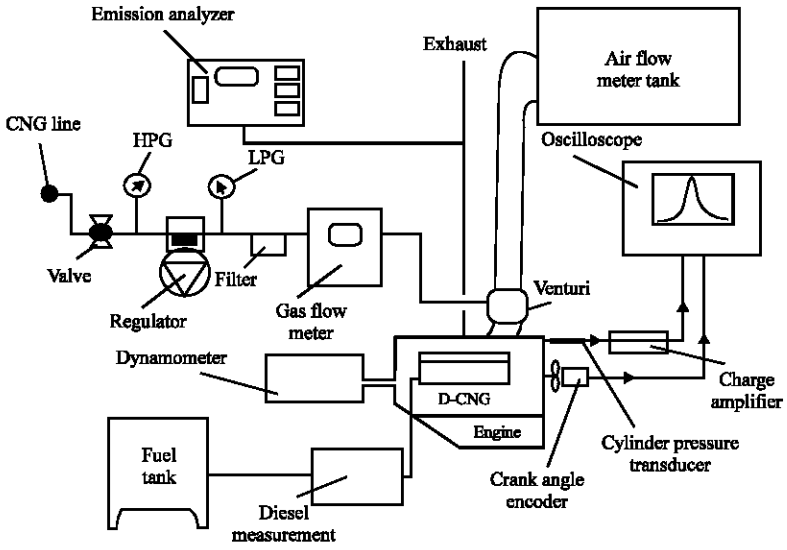

Fig. 3: Schematic of experimental setup

Table 1: OM-355 Engine specifications and operating conditions (Pirouzpanah and Saray, 2007)

Engine model	OM-355
Number of cylinders	6
Bore	128 (mm)
Stroke	150 (mm)
Compression ratio	16.1:1
Maximum torque speed	1400 (rpm)

Table 2: Test and simulation conditions performed on the engine

Case	1	2	3	4	5
Speed (rpm)	1400	1400	1400	1400	1400
Torque (Nm)	794	737	-	-	-
Inlet air temp. (K)	300	314	314	314	314
Inlet air press (kPa)	99.0	121.5	121.5	121.5	121.5
SOI (ATDC)	-18	-18.5	-18.5	-18.5	-18.5
Diesel (mg/cyc)	101	8.52	8.52	8.52	8.52
ϕ_{NG}	0	0.468	0.247	0.594	0.468
ϕ_{tot}	0.746	0.53	0.31	0.656	0.53
Piston bowl	Cyl.	Cyl.	Cyl.	Cyl.	Omega

experimental system is shown in Fig. 3. In this study, exhaust gas emissions such as NO (by signal analyzer, 4000 VM) and soot (by a Bosch smoke meter) were measured.

Table 2 shows the test and simulation conditions performed on the above mentioned engine in this research. Equation 4 and 5 show how the equivalence ratios in Table 2 are calculated (Pirouzpanah and Saray, 2007).

$$\phi_{tot} = (14.75\dot{m}_p + 15.22\dot{m}_{CNG}) / \dot{m}_a \quad (5)$$

$$\phi = \frac{(AFR)_{st}}{(AFR)_{act}} \quad (6)$$

Model formulation: Turbulent flow in the combustion chamber was modeled with k-ε turbulence model. An eddy break-up combustion model was implemented to simulate the combustion process in a diesel engine. The reaction mechanism used for the simulation of the auto-ignition of the diesel fuel is based upon an extended version of the well known SHELL model (Kong and Reitz, 1993). For the pilot fuel combustion SHELL auto-ignition model accompanied by a diesel EBU model (Magnussen and Hjertager, 1976) was implemented. And for the combustion of premixed natural gas SI EBU model was applied.

Auto-ignition model: The SHELL ignition model (Kong and Reitz, 1993) was implemented as the auto-ignition model in this study. The model uses a simplified reaction mechanism to simulate the auto-ignition of hydrocarbon fuels. The mechanism consists of eight generic reactions and five generic species. The reactions represent four types of elementary reaction steps that occur during ignition, namely, initiation, propagation, branching and termination. The five generic species include fuel, oxygen, radicals, intermediates species and branching agents. These reactions are based on the degenerate branching characteristics of hydrocarbon fuels. The premise is that degenerative branching controls the two-stage ignition and cool flame phenomena seen during hydrocarbon auto-ignition. A chain propagation cycle is formulated to describe the history of the branching agent together with one initiation and two termination reactions.

This model has been successfully applied in diesel ignition studies. It has been found that the rate-limiting

step in the kinetic path is the formation of the intermediate species and the ignition delay predictions are sensitive to the pre-exponential factor A_{fi} in the rate constant of this reaction. Therefore, the above kinetic constant is adjusted to account for fuel effects.

Combustion model: The EBU model of Magnussen and Hjertager (1976) is related to the EBU model of Spalding (1971), but has been developed assuming that in most technical applications the chemical reaction rates are fast compared to the mixing. Thus, the reaction rate is determined by the rate of intermixing of fuel and oxygen-containing eddies, i.e., by dissipation rate of the eddies. For such a case, the EBU model can be written:

$$\dot{\omega} = A\frac{\varepsilon}{k}\min\left(Y_{fuel}, \frac{Y_{oxygen}}{r_f}, B\frac{Y_{products}}{1+r_f}\right) \quad (7)$$

where, Y is the mass fraction and r_f the stoichiometric coefficient for the overall reaction written on mass basis. A and B are experimentally determined constants of the model, whereas k is the turbulent kinetic energy and ε its dissipation rate. The product dependence for the reaction rate is a deviation from the pure fast chemistry assumption, since the assumption here is that without products the temperature will be too low for reactions. This model assumes that in premixed turbulent flames, the reactants (fuel and oxygen) are contained in the same eddies and are separated from eddies containing hot combustion products (Djavareshkian *et al*., 2008).

Spray and break-up modeling: Currently the most common spray description is based on the Lagrangian discrete droplet method. While the continuous gaseous phase is described by the standard Eulerian conservation equations, the transport of the dispersed phase is calculated by tracking the trajectories of a certain number of representative parcels (particles). Various sub-models were used to account for the effects of turbulent dispersion, coalescence, evaporation, wall interaction and droplet break up (Djavareshkian and Ghasemi, 2009).

RESULTS AND DISCUSSION

Results of the diesel case (case_1): Comparison of mean cylinder pressure for present calculation in case_1 and experiments is demonstrated in Fig. 4. As can be seen, the agreement between two results is very good. Variations of mean cylinder temperature with crank angle for case_1 is shown in Fig. 5. Heat release rate diagram for case_1 is presented Fig. 6. Figure 6 exhibits diesel combustion behavior containing premixed and diffusion stages of

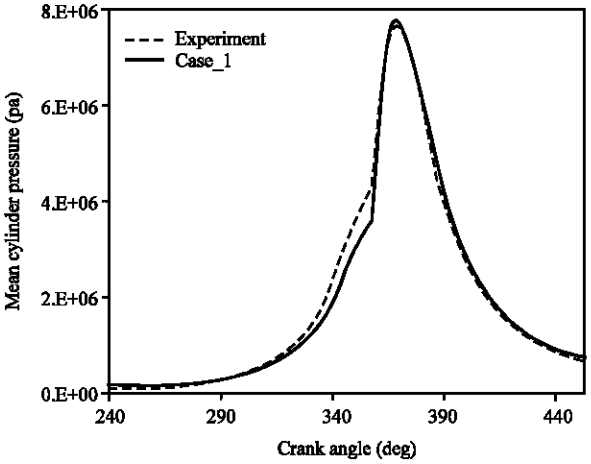

Fig. 4: Comparison of Cylinder pressure for Model in case_1 and experiment

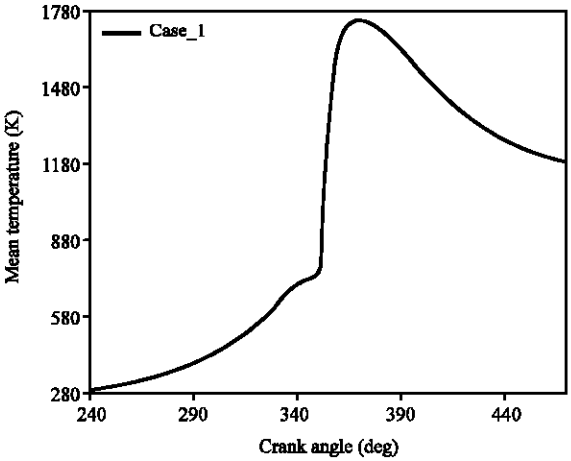

Fig. 5: Variations of mean cylinder temperature with crank angle for case_1

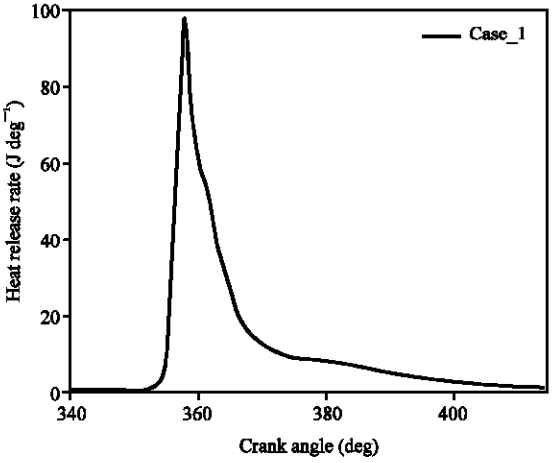

Fig. 6: Heat release rate diagram for case_1

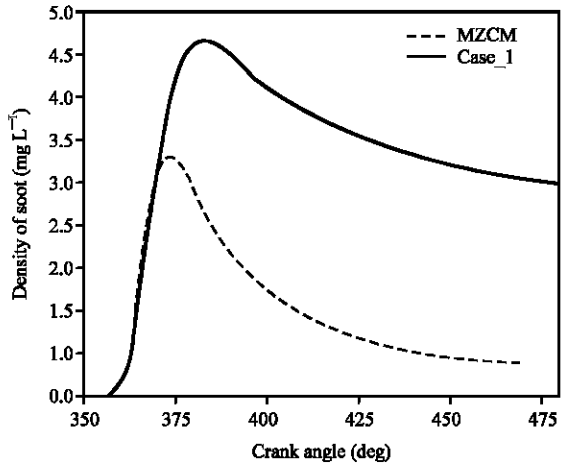

Fig. 7: Soot formation in the combustion chamber for case_1 and the MZCM (Pirouzpanah and Kashani, 2000)

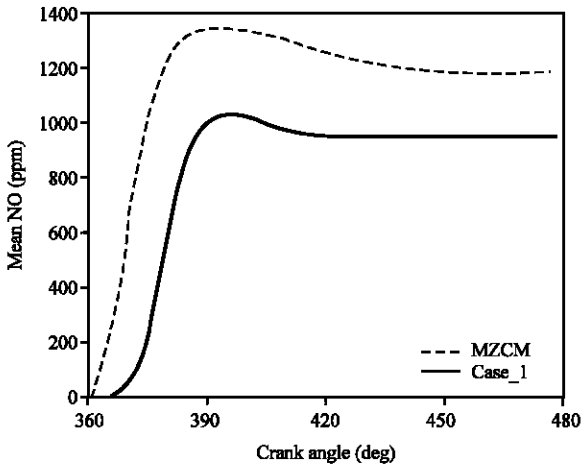

Fig. 8: NO formation in the combustion chamber for case_1 and the MZCM (Pirouzpanah and Kashani, 2000)

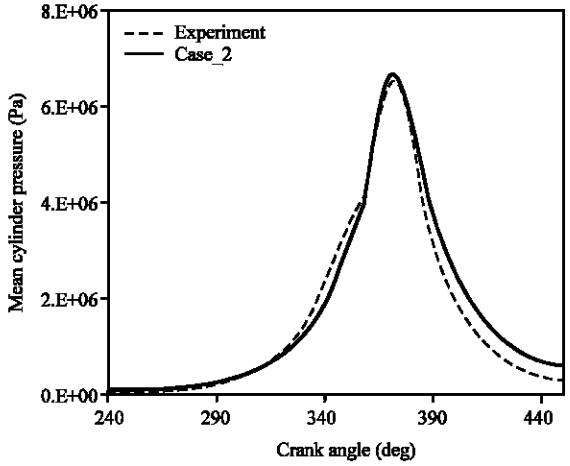

Fig. 9: Comparison of Cylinder pressure for Model in case_2 and experiments

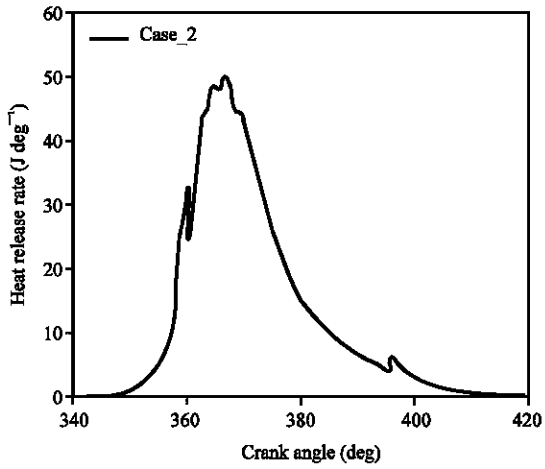

Fig. 10: Heat release rate diagram for case_2

combustion. Comparing this diagram with temperature and pressure diagrams shows high rates of temperature and pressure rise during the premixed combustion period.

Figure 7 and 8 demonstrate the history of soot and NO formation in the combustion chamber for case_1 compared to (Pirouzpanah and Kashani, 2000), the MZCM. It can be seen that most of the NO is formed during the high temperature premixed combustion and during the diffusion combustion period soot formation increases and then Oxidized.

Results of the dual fuel case (case_2): Figure 9 shows the comparison of mean cylinder pressure for present calculation in case_2 and experiment. It can be seen that good levels of agreement are obtained when using the present model. Figure 10 shows the heat release rate diagram for case_2. This shows that the model has been capable of predicting full load behavior of the heat release rate diagram.

Effect of premixed natural gas equivalence ratio (cases_2-4): Here, effect of premixed natural gas equivalence ratio on performance and pollutat formation of the dual fuel case is investigated, while the amount of pilot fuel injected remains constant. Figure 11 shows the comparison of heat release rate diagram for cases_2, 3 and 4. As it can be seen, by increasing the amount of natural gas with constant pilot fuel, the second peak in heat release rate diagram, which is related to the combustion of

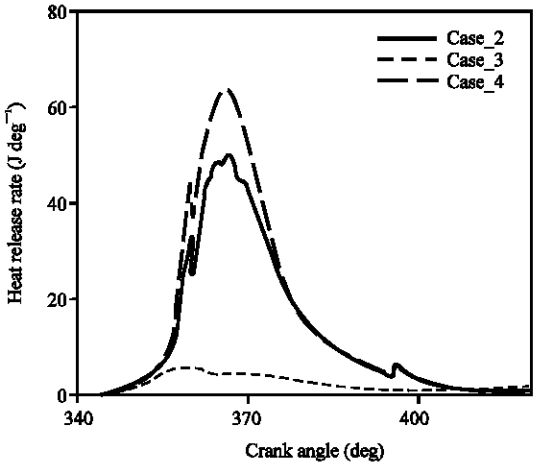

Fig. 11: Comparison of heat release rate diagram for case_2, 3 and 4

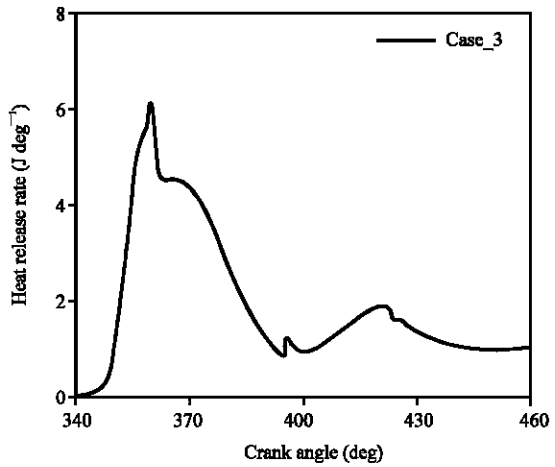

Fig. 12: Heat release rate diagram for case_3

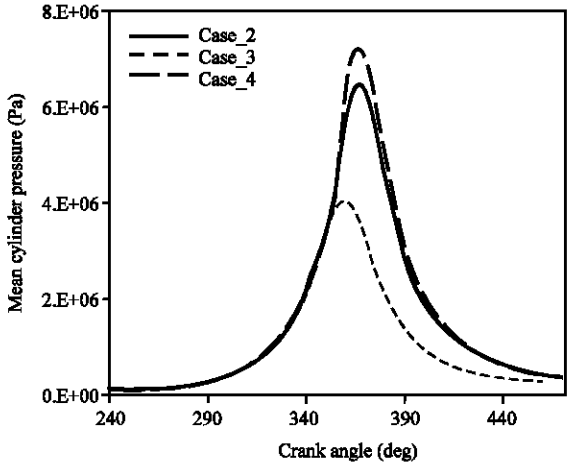

Fig. 13: Comparison of mean cylinder pressure for case_2, 3 and 4

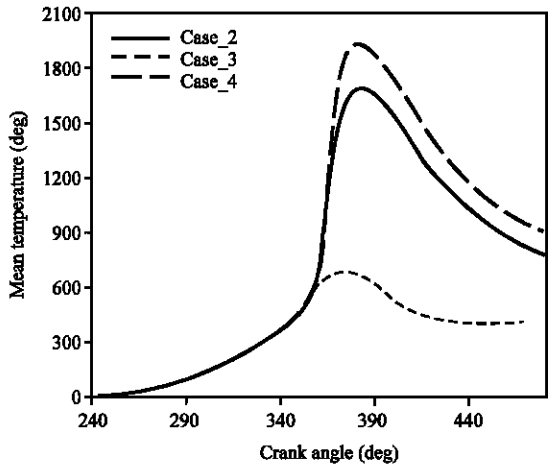

Fig. 14: Comparison of mean temperature cases_2, 3 and 4

premixed natural gas, increased and retarded. In cases_2 and 4 the heat release rate diagram exhibits full load behavior, while in case_3 it has a part load behavior with lower second peak.

The heat release rate diagram for case_3 is brought separately in Fig. 12 to represent a better display of its part load behavior. Figure 13 shows the comparison of mean cylinder pressure for cases_2, 3 and 4. Increasing premixed natural gas has lead to retarded and increased peak pressure. In case_3, very lean air/natural gas could not produce a flame propagation, so, the pressure diagram has tended to motoring condition diagram. Figure 14-16 show the comparison of mean temperature, NO and soot formation for cases_2, 3 and 4. It can be seen that more natural gas causes higher temperatures and consequently more NO formation. Although, dual fuel case has produced much lower amounts of soot compared to the diesel case but increasing natural gas lead to higher soot formation.

Comparison of laminar flame speed contours for cases_2, 3 and 4, in 375, 380, 430 and 460 CA degree is illustrated in Fig. 17a-*l*. In cases_2 and 4, ignition begins in a near stoichiometric region at the tip of the fuel jet and as it can be seen, this region provides a flame core in the piston bowl. This flame core initiates a propagating flame which spreads through the air/natural gas mixture in other regions of the combustion chamber during the expansion. When the flame reaches the cold walls it begins to quench. On the other hand, the very lean premixed condition of air/natural gas mixture in case_3, prevents the formation of a propagating flame and this causes some

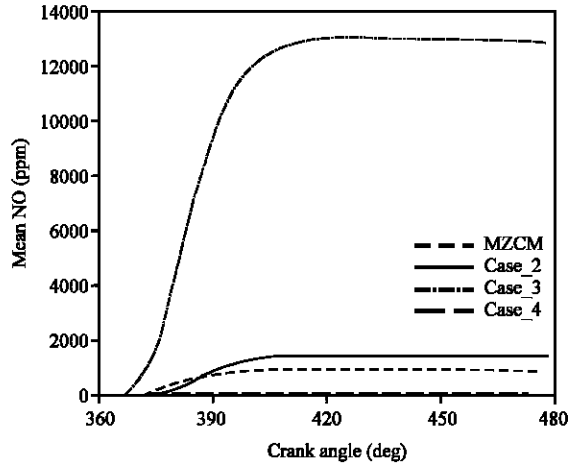

Fig. 15: NO formation for case_2, 3, 4 and the MZCM (Pirouzpanah and Kashani, 2000)

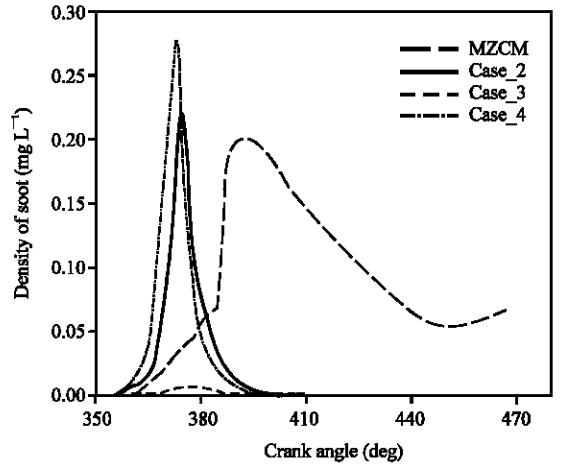

Fig. 16: Comparison of soot formation for case_2, 3, 4 and the MZCM (Pirouzpanah and Kashani, 2000)

gaseous fuel to remain unburnt. It is obvious that the lamiar flame speed is greater in near stoichiometric regions and has lower values in very lean and very rich regions.

Effect of piston bowl shape (cases_2, 5): For case_5 all the conditions are the same as the case_2, except for the piston bowl shape. In order to take into account the piston bowl shape in combustion chamber flow field and its subsequent effect on dual fuel engine performance and emissions, a reentrant OMEGA piston type is used in case_5. Figure 18 shows the comparison of mean cylinder pressure for case_2 and 5. Figure 19 shows the comparison of heat release rate diagram for case_2 and 5. it seems that case_5 represents a long, smooth and low pressure combustion, compared to case_2, in the premixed natural gas combustion phase.

Figure 20 and 21 show the comparison of mean temperature and NO formation for cases_2 and 5. high temperature and oxygen availability are two important factors in NO formation, here for case_2 the second factor is dominant because of the higher swirl flow near TDC.

Figure 22 shows the comparison of soot formation for case_2 and 5, in case_5 lack of available oxygen, because of lower swirl motion, caused more soot formation. Figure 23 shows the comparison of swirl motion for case_2 and 5. the reason for higher swirl near TDC is because of the concentration of the high momentum mass in the small volume of the piston bowl. because of the smaller bowl diameter and lower bowl volume, case_2 has more swirl ratio near TDC. Since, case_5 is a reentrant type it provides more durable swirl motion till the end of combustion, while there is a severe falling of swirl for case_2 after TDC.

Figure 24 shows the comparison of Sauter Mean Diameter (SMD) for case_2 and 5. this parameter can be as a criterion for a successful breakup process in the combustion chamber, which can affect ignition delay and accordingly combustion, engine performance and emission. In case_2, higher swirl motion exerts stronger aerodynamic effects on droplets, therefore it has a smaller penetration and breakup time. For both cases, at the end of the process SMD increases slightly for a while because of the coalescence. An x-y half stroke cut for velocity vectors for cases_2 and 5, at 355, 365 and 375 CA degree is shown in Fig. 25a-h. It can be seen that flowfield consists of a circumferential and a radial pattern. The flow vectors in the radial flow pattern are towards the cylinder axis before TDC and in a reverse direction after TDC. These vectors become maximum in a particular radius and are greater for case_2.

An y-z cut for velocity vectors for cases_2 and 5, at 355, 360, 365 and 375 CA degree is shown in Fig. 26a-f. Vortex prediction at the corners of the flowfield, specialy for case_2, verifies appropriate grid size and model capability. It can be seen that velocity vectors adjacent to the wall are parallel to it. So, the governing flow in the piston bowl is of rotating type. By paying more precise attention to velocity vectors, it can be seen that in addition to tangential terms (rotating flow), they also have axial and radial terms and these terms together produce 3D vortices in the piston bowl. Before TDC the influence of squish is becoming apparent above the bowl and almost dominates the flow of all gas fields above the bowl. But near TDC, as the speed of piston tends to zero, squish above the bowl decreases. In the bowl, a single toroidal vortex has been formed. After TDC, above the bowl, reverse squish has formed. In the bowl, however, the toroidal vortex is still in keeping with that at TDC in the

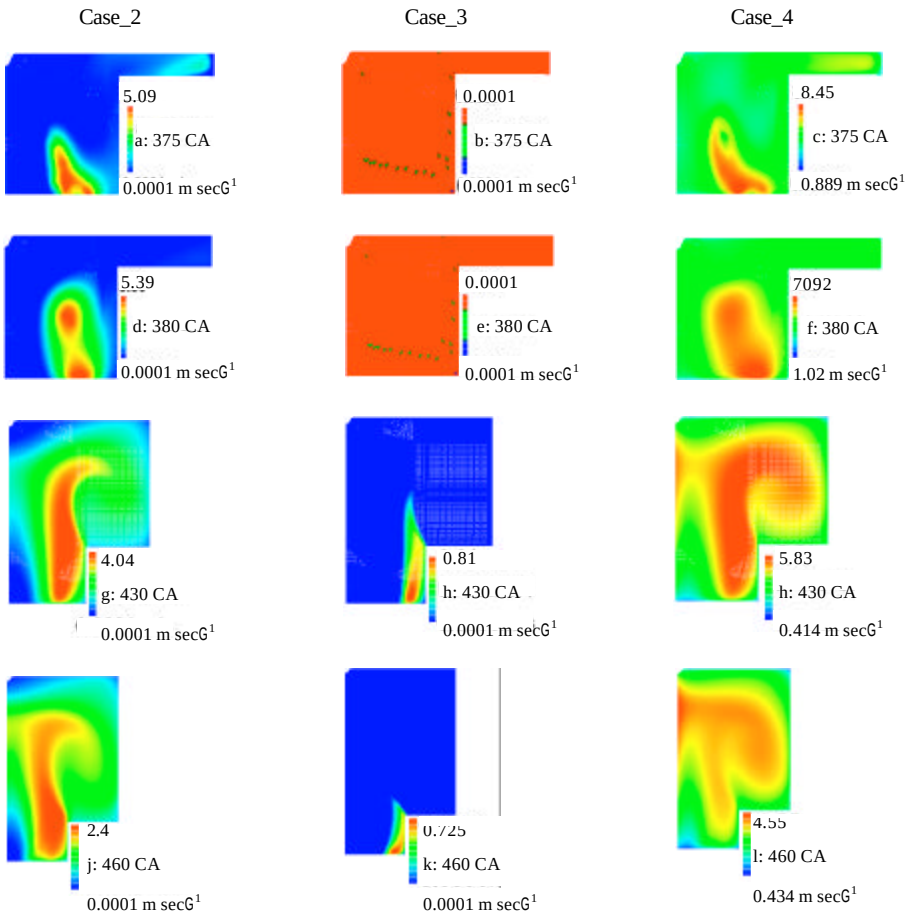

Fig. 17: (a-*l*) Comparison of laminar flame speed contours for case_2, 3 and 4, in 375, 380, 430 and 460 CA degree

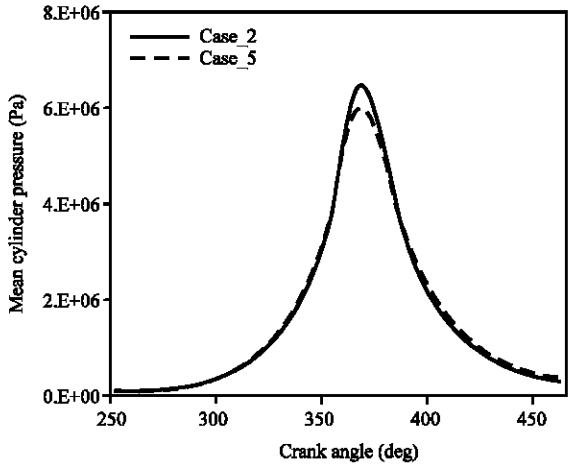

Fig. 18: Comparison of mean cylinder pressure for case_2 and 5

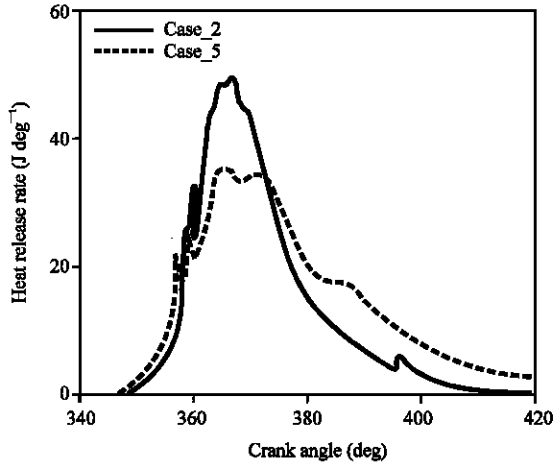

Fig. 19: Comparison of heat release rate diagram for case_2 and 5

way of its shape and intensity. At the moment that the piston is speeding up toward BDC, the toroidal vortex is almost absent in the bowl, the main flow is dominantly reverse squish toward the top of piston. The toroidal

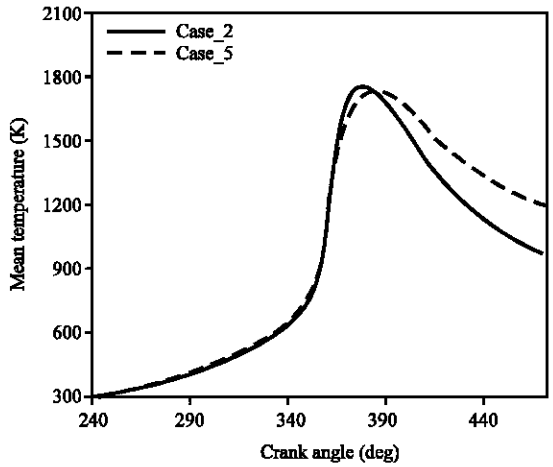

Fig. 20: Comparison of mean temperature for case_2 and 5

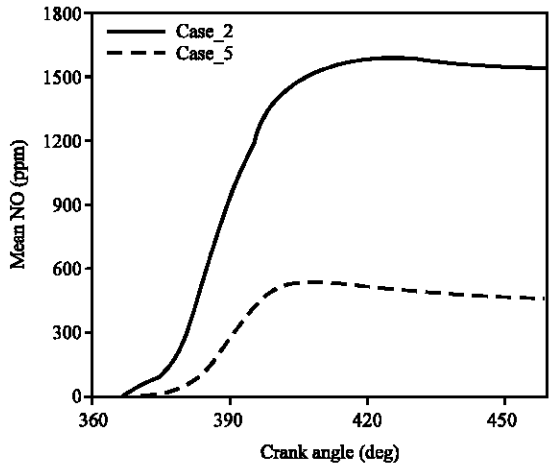

Fig. 21: Comparison of NO formation for case_2 and 5

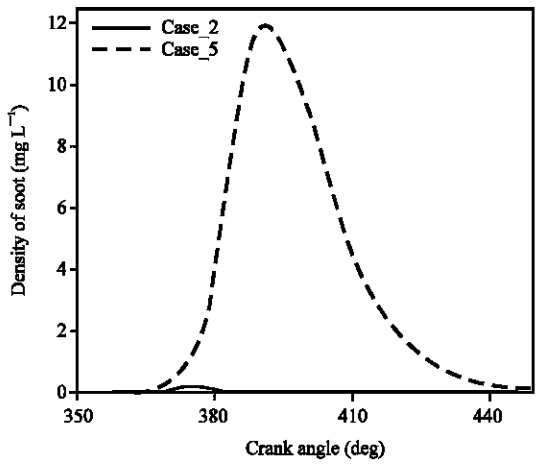

Fig. 22: Comparison of soot formation for case_2 and 5

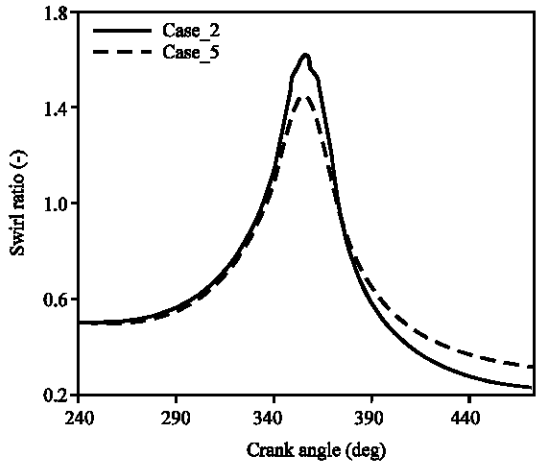

Fig. 23: Comparison of swirl motion for case_2 and 5

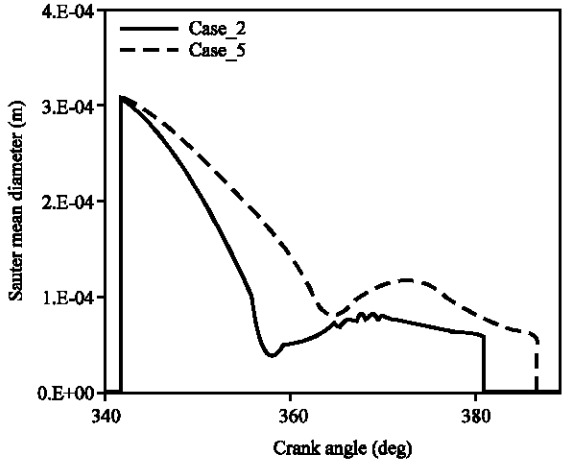

Fig. 24: Comparison of Sauter Mean Diameter for case_2 and 5

vortex is weakening enormously. In case_2 there are greater values for squish and vortex velocities.

Main results: From the study on the above mentioned cases on dual fuel engine modeling, the following conclusions may be drawn:

- The research and its comparison to previously done project on the same engine (Pirouzpanah and Kashani, 2000), demonstrated that multidimensional modeling is useful for engine modeling in diesel fuel and in dual fuel mode for different amounts of natural gas and different piston bowl geometries
- For different amounts of natural gas, model was capable of predicting full load and part load behavior

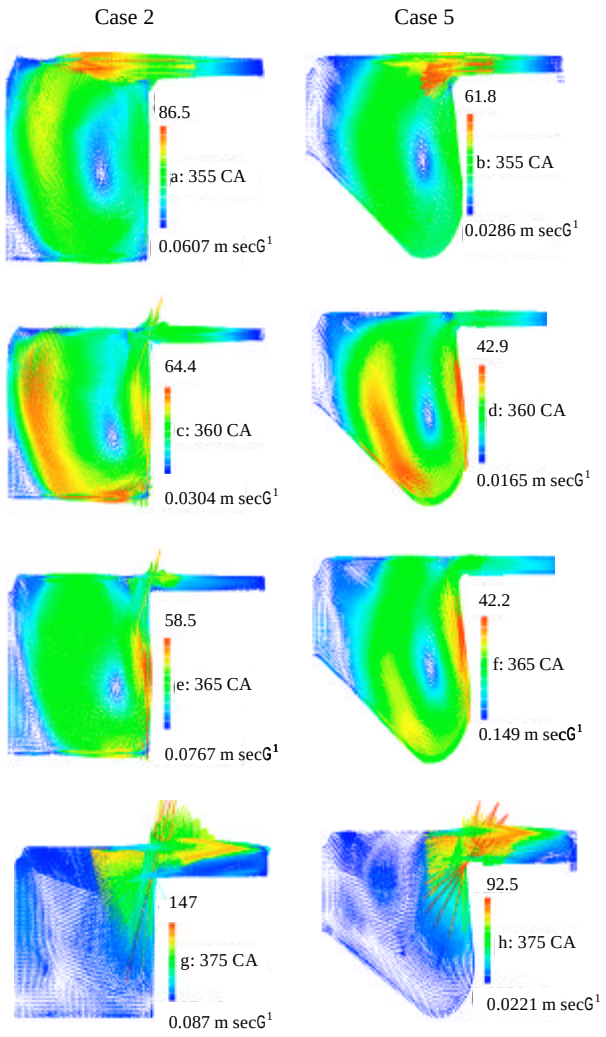

Fig. 25: (a-h) y-z cut for velocity vectors for case_2 and 5, at 355, 360, 365 and 375 CA degree

of heat release rate diagram. by increasing the amount of natural gas with constant pilot fuel, the second peak in heat release rate diagram, which is related to the combustion of premixed natural gas, increased and retarded. Increasing premixed natural gas has lead to retarded and increased peak pressure

- Increasing natural gas caused higher temperatures and consequently more NO formation. Although dual fuel case has produced much lower amounts of soot compared to the diesel case, but increasing natural gas lead to higher soot formation
- Very lean premixed condition of air/natural gas mixture in case_3, prevented the formation of a propagating flame and this caused some gaseous fuel to remain unburnt

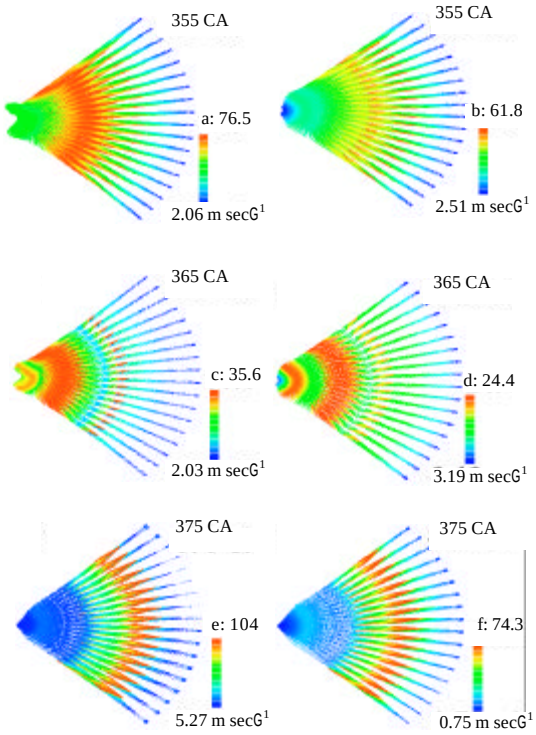

Fig. 26: (a-f) x-y half stroke cut for velocity vectors for case_2 and 5, at 355, 365 and 375 CA degree

Table 3: A comparison among simulated parameters, experiments and results of the MZCM (Pirouzpanah and Kashani, 2000)

Parameters	Diesel (CASE 1)		Dual fuel(CASE 2)	
NO (ppm)	Expt.	1060	Expt.	2130
	MZCM	1250	MZCM	1050
	Case_1	1035	Case_2	1587
Soot (Bosch NO.)	Expt.	3.42	Expt.	0.52
	MZCM	4.94	MZCM	0.47
	CASE_1	2.81	Case_2	0.51

- Higher swirl flow and accordingly more available oxygen, lead to more NO formation and less soot formation of case_2 than case_5
- Case_2 had greater values of squish and vortex velocities, in comparison with case_5

CONCLUSION

In the present study the multi-dimensional combustion modeling was carried out for diesel fuel mode and dual fuel mode. Also flow field simulation was performed for two different piston bowls in dual fuel mode. Results were validated via experiments for OM_355 DI diesel engine in diesel and dual fuel modes. Table 3 provides a comparison among some parameters, in this calculation, experiments and results of the (Pirouzpanah

and Kashani, 2000) for the same engine using MZCM. It can be inferred from the results that CFD simulations led to more accurate prediction of No and Soot formation. There have been good agreements between experiments and the CFD calculations.

ACKNOWLEDGMENT

The researchers are indebted to professor V. Pirouzpanah for his collaboration during this research and for preceding works he had done. We wish to thanks all the compassionate sacrifices he made throughout his valuable life, until the last moments of his departure.

NOMENCLATURE

U	=	Velocity
P	=	Pressure
H	=	Enthalpy
T	=	Temperature
C	=	Species concentration
k	=	Turbulent kinetic energy
$\dot{m}$	=	Mass flow rate
Y	=	Mass fraction
r_f	=	Stoichiometric coefficient

Greek symbols

$\hat{\rho}$	=	Density
μ	=	Viscosity
ϕ	=	Equivalence ratio
$\dot{\omega}$	=	Combustion reaction rate
ε	=	Turbulent dissipation rate

Subscripts

p	=	Pilot
a	=	Air
st	=	Stoichiometric
act	=	Actual

Abbreviations

DI	=	Direct injection
SI	=	Spark ignition
MZCM	=	Multi zone combustion model
CFD	=	Computational fluid dynamics
CA	=	Crank angle
TDC	=	Top dead center
EBU	=	Eddy break-up
CNG	=	Compressed natural gas
AFR	=	Air/fuel ratio
SOI	=	Start of injection

REFERENCES

Badr O., G.A. Karim and B. Liu, 1999. An examination of the flame spread limits in a dual fuel engine. Applied Thermal Eng., 19: 1071-1080.

Djavareshkian, M.H., F. Talati, A. Ghasemi and S. Sohrabi, 2008. Multidimensional combustion simulation and analytical solution of wall heat conduction in di diesel engine. J. Applied Sci., 8: 3806-3818.

Djavareshkian, M.H. and A. Ghasemi, 2009. Investigation of jet break-up process in diesel engine spray modelling. J. Applied Sci., 9: 2078-2087.

Hountalas, D.T. and R.G. Papagiannakis, 2001. A simulation model for the combustion process of natural gas engines with pilot diesel fuel as an ignition source. SAE Trans., 110: 1496-1509.

Karim, G.A., Z. Liu and W. Jones, 1993. Exhaust emissions from dual fuel engines at light loads. http://www.sae.org/technical/papers/932822.

Kong, S.C. and Reitz, R.D., 1993. Multidimensional modeling of diesel ignition and combustion using a multi-step kinetics model. J. Eng. Gas Turbines Power, 115: 781-781.

Magnussen, B.F. and B.H. Hjertager, 1976. Sixteenth Symposium (International) on Combustion. Combustion Institute, Pittsburgh, PA., pp: 719-729.

Pirouzpanah V. and K.R. Saray, 2007. Comparison of thermal and radical effects of EGR gases on combustion process in dual fuel engines at part loads. Energy Convers. Manage., 48: 1909-1918.

Pirouzpanah V. and Kashani B.O., 2000. Prediction of major pollutants emission in direct - injection dual-fuel diesel and natural-gas engines. Int. J. Eng., 13: 55-67.

Satbir, S., L. Liang, S.C. Kong and R.D. Reitz, 2006. Development of a flame propagation model for dual-fuel partially premixed compression ignition engines. Int. J. Engine Res., 7: 65-75.

Singh, S., S.C. Kong, R.D. Reitz, S.R. Krishnan and K.C. Midkiff, 2004. Modeling and experiments of dual-fuel engine combustion and emissions. SAE Trans., 113: 124-133.

Spalding, D.B., 1971. Thirteenth Symposium (International) on Combustion. Combustion Institute, Pittsburgh, PA., pp: 649-657.

Yasuhiro, D., T. Kou, I. Yuki, N. Shigeki, K. Ryoji and S. Takeshi, 1995. Controlling combustion and exhaust emissions in a direct-injection diesel engine dual-fueled with natural gas. SAE Paper SAE 952436.